SEMARAK ILMU PUBLISHING

Journal of Advanced Research in Applied Mechanics

Journal homepage:
https://semarakilmu.com.my/journals/index.php/appl_mech/index
ISSN: 2289-7895

Electronic and Topological Properties of UIO66-ILs Interaction through a Computational Study

Nor Ain Fathihah Abdullah[1], Lim Jun Wei[1], Khairulazhar Jumbri[1,*]

[1] Department of Fundamental and Applied Science, Universiti Teknologi Petronas, Perak, Malaysia

ARTICLE INFO

Article history:
Received 5 December 2022
Received in revised form 23 January 2023
Accepted 30 January 2023
Available online 15 February 2023

Keywords:
Binding energies; molecular docking; metal-organic framework; ionic liquid; adsorbent

ABSTRACT

A high surface area adsorbent, such as MOFs, is an attractive option to evacuate heavy metals from wastewater. However, due to the possibility of the MOF structure collapsing when exposed to water, the stability and selectivity of MOFs for wastewater treatment remain a debatable task. Depending on the application, it has been shown that the consolidation of IL into MOF could improve the stability and reusability of pure MOF; nevertheless, research on the molecular interactions between the MOF framework and IL is still lacking. The stability, compatibility, and selectivity of this hybrid material are significantly influenced by the fundamental interactions between the MOFs and ILs moieties (cation and anion molecules), particularly the sorts of interactions. In this work, we focused on the topological properties of ILs and utilization of molecular docking calculations to assess the binding energy (ΔGbind) and binding affinity between UIO66 with TFSI-imidazole and TFSI-pyridinium ILs studied. The properties of ILs such as aromaticity of the structures, bond critical point (BCP), and electrostatic potential map surface were carried out using the Gaussian and Multiwfn software while the binding energies were computed using the AutoDock software to identify particular binding sites for IL toward MOF. The Autodock software's default setting was used to prepare all of the structures. To determine the binding locations of MOF, the IL was successively incorporated into the MOF pores inside the grid box of 90 x 90 x 90 Å (x, y, and z) dimensions. The results showed that both ILs; TFSI-imidazole, and TFSI-pyridinium IL, interacted favorably with the MOFs, having binding energies varying from -4.12 to -8.60 kcal mol^{-1}. The stability of UIO66-ILs system increases with the addition of anion and cation. According to docking molecular structures, both cation and anion tend to bind in the corner of the MOF pore, which is in line with the previous work.

1. Introduction

Water is an indispensable substance for living organisms. One of the most formidable sustainability issues faced throughout the world is safe water resources. The contamination of water by hazardous contaminants such as heavy metal ions due to intensive industrial activities deteriorated the quality of available water resources. The discharge of these heavy metals into water

* *Corresponding author.*
E-mail address: khairulazhar.jumbri@utp.edu.my

https://doi.org/10.37934/aram.102.1.4453

sources can cause a destructive effect on the ecological balance of humans as well as animal life. The high amount of heavy metals exposure to living organisms (including humans) can lead to poisonings, life-threatening, and promotes a variety of physiological disorders. Therefore, the removal of heavy metals from industrial wastewater streams continues to be a challenge using today's wastewater treatment technologies [1-3].

Nowadays, the emergence of using MOFs in water treatment has become a topic of interest. MOFs have been considered one of the compelling adsorbents to evacuate overwhelming metal from water sources [4-6]. Their high porosities, tunable structures, and convenient process of presenting both customizable functional groups and unsaturated metal centers have managed great adsorption capacity. Despite this, the systems may collapse upon introduction to dampness making the stability of the MOFs questionable [7-9]. The framework is depending on its metal-ligand interaction which is vulnerable to ligand substitution by water or other nucleophiles. The collapsed structure of MOF upon adsorption of water will create another metal defilement as the metal in MOF is discharged into the watery medium. This can be a genuine concern in wastewater treatment as the interaction of MOF and water can lead to the flimsiness of MOF. Whether the MOFs seem completely keep up their capacities and basic structure after multicycle applications require advanced examination. The MOF5, UIO66, and ZIF8 are some examples of MOFs that have large surface areas. The strong coordination bonds between metal and organic ligands of MOF make it stable in acidic or alkaline conditions. This provides the relevance of applying these MOFs in wastewater treatment.

Recent studies have suggested that the hybridization of a MOF with a different component may result in novel materials that share traits with both the host MOF and the component that was introduced. A new kind of "designer hybrid material" with improved host MOF properties could result from this combination in a variety of applications. These hybrid MOFs have demonstrated promising results in various applications such as catalysis [10], gas and separation [11, 12], energy storage [13], and electrochemical [14]. Previously, the encapsulated ILs into MOF give great performance, especially in gas adsorption [15, 16]. It had been proven that the performance of MOFs incorporated with ILs had been improved especially in their stability and reusability, depending on the particular applications.

The consolidation of IL into MOFs pores to remove contaminants, especially heavy metals from wastewater, is a growing research area. Despite having been evidenced to be a resultful strategy for enhancing the performance of pristine MOF, the interaction and their fundamentals are not well explored. There are several interaction sites and functional groups in both MOFs and ILs. As a result, more intricate interaction systems are involved, including hydrogen bonds, van der Waals interactions, polarization, and Coulumbic forces (electrostatic attraction or repulsion) [17, 18]. Therefore, understanding their individual properties is of utmost importance as it could help to form a specific type of MOF-IL hybrid adsorbent. It is still a significant challenge, but more research into the particular interaction between IL and MOF might improve the performance of these IL-MOFs type hybrid materials.

In pursuance of identifying the effect of the confinement ILs on MOFs stability, herein, in this paper, we reported the comparison between pristine UIO66 and UIO66-ILs by binding energy calculation. The other details on the MOFs dynamic properties and their interaction with ILs also were investigated using molecular dynamic (MD) simulation and will be disclosed in the next paper.

2. Methodology

To determine the binding energy and binding affinity of small compounds that bind to certain receptor binding sites, molecular docking calculation was carried out. From the Automated Topology

Builder (ATB) [19] web database, the starting structures of the ILs; 1-ethyl-3-methylimidazolium (EMIM), 1-propyl-3-methylimidazolium (PMIM), 1-butyl-3-methylimidazolium (BMIM), 1-ethyl-4-methylpyridinium (EMPYDM), 1-propyl-4-methylpyridinium (PMPYDM), 1-butyl-4-methylpyridinium (BMPYDM), and bis((trifluoro)sulfonyl)imide (TFSI), are obtained. These structures have been optimized at B3LYP/6-31G* level theory. To be utilized later for docking calculations, all of the molecules were prepared and saved in the PDBQT file type. Using the scoring mechanism to determine the optimum binding mode, the autogrid and autodock computations were executed as part of the docking simulation using the default option in AutoDock 4.2 software [20]. Each MOF-IL system was prepared by introducing each cation and anion into the macromolecular receptors cavity of UIO66 consecutively inside a grid box of 90 x 90 x 90 Å with a 0.375 Å grid spacing (as shown in Figure 1). We used the Lamarckian Genetic Algorithm (LGA) from MGLTools to determine the proper binding modes and conformation for ILs [21].

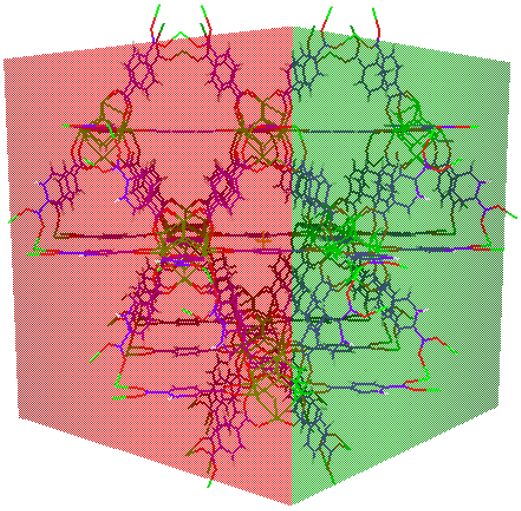

Fig. 1. The grid box of x, y, z (90 x 90 x 90 Å) UIO66 docked with ILs

The following equation was then used to determine the binding energy (ΔG_{bind}) of the inclusion complex

$$\Delta G_{bind} = \Delta G_{VDW} + \Delta G_{elect} + \Delta G_{Hbond} + \Delta G_{desolv} + \Delta G_{tor} \quad (1)$$

where ΔG_{VDW} represents van der Waal energy, ΔG_{elect} refers to electrostatic energy, ΔG_{HBond} is hydrogen bonding energy, ΔG_{desolv} is desolvation energy and ΔG_{tor} refers to torsional free energy.

The total density and electrostatic potential of ILs were generated using GaussView [22] to determine the localization of electrons of the molecules. Then, the topology (bond critical points and aromaticity) of the imidazole and pyridinium were analyzed using Multiwfn software [23]. The aromaticity of the ILs was then calculated based on the Shannon aromaticity (SA) index [24]. The formula can be briefly written as,

$$SA = \ln(N) + \sum_{i}^{N} (-p_i \ln p_i) \quad (2)$$

$$p_i = \frac{\rho(\mathbf{r}_{BCPi})}{\sum_i^N \rho(\mathbf{r}_{BCPi})} \tag{3}$$

where N is the total number of BCPs in the ring, $\mathbf{r}_{BCP}$ is the position of BCP, and p_i refers to the estimated normalized probability of the occurrence of specific data.

3. Results and Discussion

3.1 Topological Properties of ILs

The inclusion of ILs inside MOF has shown great potential in various fields. The investigation of finding matching ILs with MOF is important to ensure the performance of this hybrid material could enhance this specific type-MOF. In this work, the specific topological properties of TFSI-imidazole and TFSI-pyridinium-based-ILs were investigated to find the possible locations interaction of ILs toward MOF. To determine the electronic and topological properties of ILs, the map electrostatic potential (MEP) was generated by GaussView and Multiwfn software and are illustrated in Figure 2 and 3, respectively. Since the structures of imidazole (EMIM, PMIM, BMIM) and pyridinium (EMPYDM, PMPYDM, BMPYDM) have similar geometry, the MEP surface was only plotted for one structure from each type, respectively. MEP surface enables visualization of charge distribution throughout the molecules using colour codes. The region filled with red colour indicates more negative potential, while the area shaded with blue color indicates less negative potential (or positive potential).

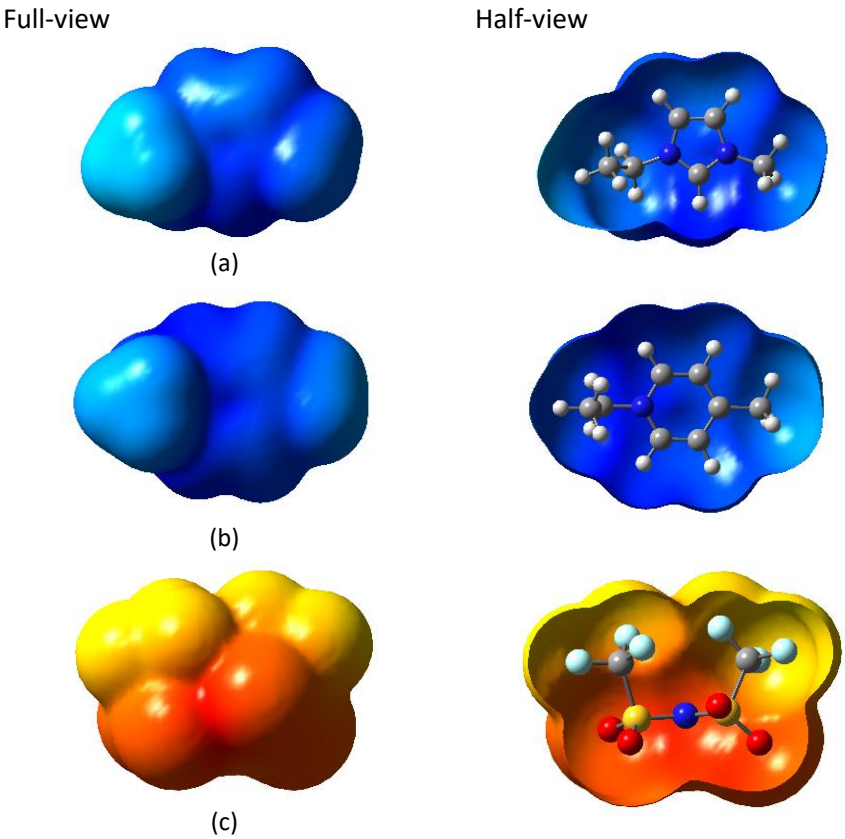

Fig. 2. The electrostatic potential map of (a) EMIM (b) EMPYDM (c) TFSI. Atoms C, H, N, O, F, and S are colored grey, white, blue, red, turquoise, and orange, respectively

In Figure 2, the MEP surface of ILs is portrayed in two views; full-view and half-view, to make it easier to locate the color distribution of the atoms. Both imidazole (EMIM) and pyridinium (EMPYDM) are shaded with the blue region which elucidates their positive potential in that particular region. The distribution of positive potential in the blue region is strongly contributed by carbon and hydrogen atoms. In contrast, a higher negative potential was observed in TFSI. The most negative potential is distributed around oxygen and sulfur (red region) while fluorine exhibits less negative potential (orange region) than sulfur and oxygen. The red region represents the negative potential associated with electrophilic sites, while the blue region represents the positive potential which is suitable for the nucleophilic attack [25]. From these properties, the possible locations of ILs interacting with MOF were identified for further calculation.

The topological analysis based on electron density at the wave function generated at B3LYP/6-31G* level of theory was then carried out. The bond critical point (BCP) for the imidazole and pyridinium structures was discovered using Atom-in-molecules (AIM) study. BCP is the location where two neighboring atoms meet, defining the atoms' bonding. The local information at this critical point is a good indicator to determine the aromaticity of the structures. Figure 3 shows where the BCP (orange dots) was located in the imidazole and pyridinium ILs. Notably, the little orange dots on the bond show the presence of the BCP between C-C, C-H, and C-N bonds which demonstrates that between these bonds the electron density has effectively built up.

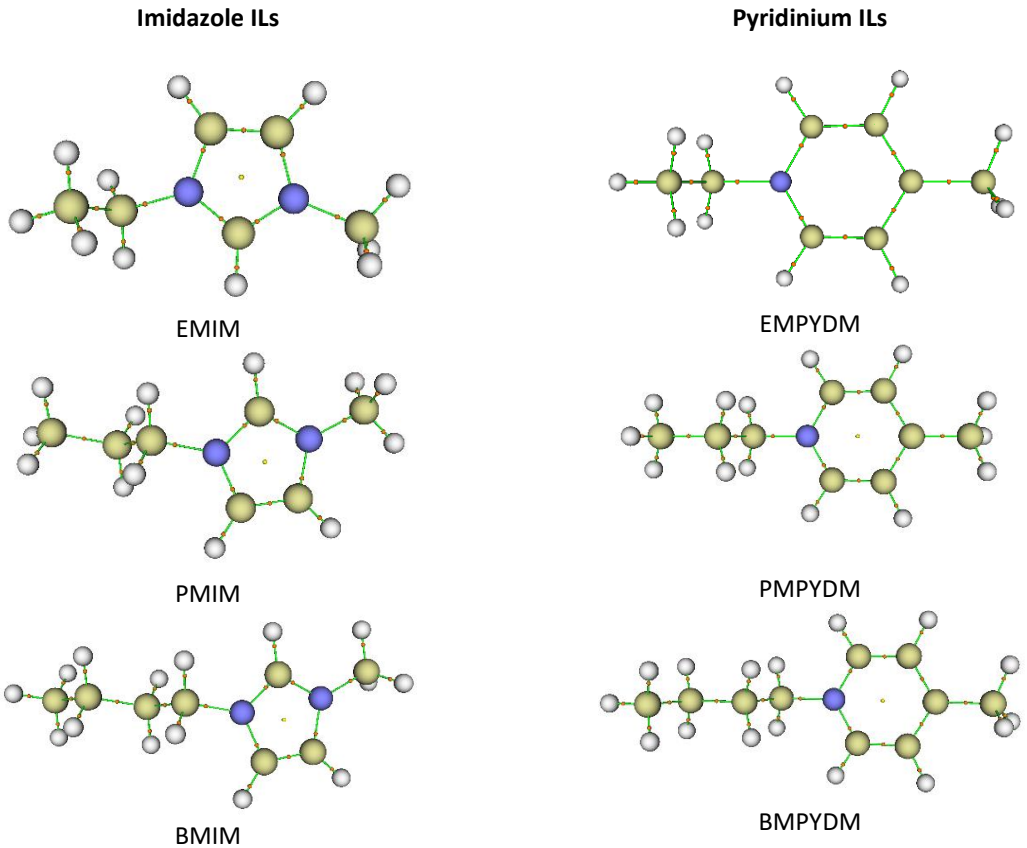

Fig. 3. Positions of the BCP (orange dot) critical points in imidazole (EMIM, PMIM, BMIM) and pyridinium (EMPYDM, PMPYDM, BMPYDM) ILs. Atoms C, H, and N are colored yellow, white, and blue, respectively

The aromaticity of imidazole and pyridinium was then determined using the Shannon aromaticity index (SA) which had been proposed by the Norizadeh groups [24]. The aromaticity value was identified based on electron density at BCPs in the ring (as shown in Figure 3) and was tabulated in

Table 1. According to the report, the boundary between the aromatic and non-aromatic compounds was found to be 0.003 < SA < 0.005, respectively. The smaller the SA index, the more aromatic is the ring. In this work, all the SA values obtained are less than 0.003 (refer to Table 1), which denoted the aromaticity character for both molecules. The value of pyridinium aromaticity was found to be significantly smaller compared to imidazole IL. These results show that pyridinium exhibits a strong aromaticity character than imidazolium, thus making pyridinium have a more stable structure.

In previous work, Kruszewski and Krygowski [26] have come out with the idea of using the Harmonic Osilator Model of Aromaticity (HOMA) method to determine the aromaticity of the compound. This method has been used as a reference by researchers until today [27-29]. The HOMA value for pyridinium was found to be closer to the unity value (~1) than imidazole [30]. The closer the HOMA value to ~1, the stronger the aromaticity character of the compound. Thus, the aromaticity result obtains in this work agrees with the previous work.

Table 1
The aromaticity index (SA) for imidazole and pyridinium ILs

ILs	Cations	SA index
Imidazole	EMIM	0.001476
	PMIM	0.001469
	BMIM	0.001495
Pyridinium	EMPYDM	0.0001465
	PMPYDM	0.0001449
	BMPYDM	0.0001462

3.2 Molecular Docking

Molecular docking calculation was carried out to identify the binding interaction between ILs and UIO66. In our previous paper [31], we reported the interaction of TFSI-imidazole and TFSI-pyridinium ILs with the three MOFs (MOF5, ZIF8, and UIO66). Among the three MOFs studied, the UIO66 exhibit a great performance in term of binding energy when interacting with both imidazole and pyridinium ILs (as shown in Table 2). The stability of the system is indicated by the binding energy's (ΔG_{bind}) negative value. The highest stability of the complex is implied by the large negative value of binding energy [32]. From the results, the UIO66 framework profoundly gave the highest binding interaction towards pyridinium-based ILs which makes it the most stable system. Herein, in this report, we focused on UIO66 binding interactions with ILs and the comparison of pristine UIO66 before and after adding cation and anion consecutively inside the UIO66 pore.

Table 2
Binding energies (ΔG_{bind}) of TFSI-imidazole and TFSI-pyridinium with UIO66 [31]

MOF	ILs	Binding Energies (kcal mol^{-1})
UIO66	EMIM-TFSI	-4.25
	PMIM-TFSI	-4.18
	BMIM-TFSI	-4.18
	EMPYDM-TFSI	-4.12
	PMPYDM-TFSI	-8.60
	BMPYDM-TFSI	-4.19

The comparison of ΔG_{bind} of UIO66 with the addition of cation and after adding both cation and anion were highlighted in Table 3. In general, the binding energies increase significantly for both UIO66-imidazole and UIO66-pyridinium after the addition of an anion to the UIO66-cation system. The addition of anion into the UIO66-cation system increases the stability and binding energy interaction of the whole system, thus making the interaction between the MOF and IL are getting stronger. In addition, it is interesting to note that the values of ΔG_{bind} for cation pyridinium (EMPYDM, PMPYDM, BMPYDM) interact with UIO66 was found to be slightly higher (-3.04 to -3.36 kcal mol^{-1}) than cation imidazole (EMIM, PMIM, BMIM) (-2.22 to -2.61 kcal mol^{-1}). This might be related to the aromaticity strength of the cations. The stronger aromaticity character of pyridinium presumably accounts for the remarkable stability in the UIO66-pyridinium system.

Table 3
Comparison of binding energies (ΔG_{bind}) of UIO66 with cation and after adding anion (TFSI)

Cation	Binding Energies, ΔG_{bind} (kcal mol^{-1})	Cation-Anion	Binding Energies, ΔG_{bind} (kcal mol^{-1})
EMIM	-2.22	EMIM-TFSI	-4.25
PMIM	-2.43	PMIM-TFSI	-4.18
BMIM	-2.61	BMIM-TFSI	-4.18
EMPYDM	-3.04	EMPYDM-TFSI	-4.12
PMPYDM	-3.23	PMPYDM-TFSI	-8.60
BMPYDM	-3.36	BMPYDM-TFSI	-4.19

To identify the preferred locations for ILs to bind inside UIO66, the molecular structure of the lowest energy conformer from docking, which is between UIO66 and PMPYDM-TFSI ILs was acquired and shown in Figure 4. The lowest energy conformer is defined by the lowest interaction energy between the cations/anions and UIO66 (high negative value). As shown in Figure 4, TFSI and PMPYDM opted to bind at various pores of UIO66 and were separated from one another. The anion and cation were located close to the metal sites in the corner of the pore, which is consistent with a prior work in which the author employed ILs of smaller size [33, 34]. Generally, the modest size of ILs encouraged stability and robust interaction with MOF [35]. In addition, the TFSI was bent more towards the metal Zr atom of UIO66. This can be understood from MEP analysis where TFSI exhibits higher negative potential associated with the electrophilic sites (refer to Figure 2).

Atoms C, H, O, and Zr are colored purple, grey, red, and blue turquoise, respectively (UIO66). Atoms C, H, O, N, S, and F are colored green, white, red, blue, yellow, and green turquoise (ILs).

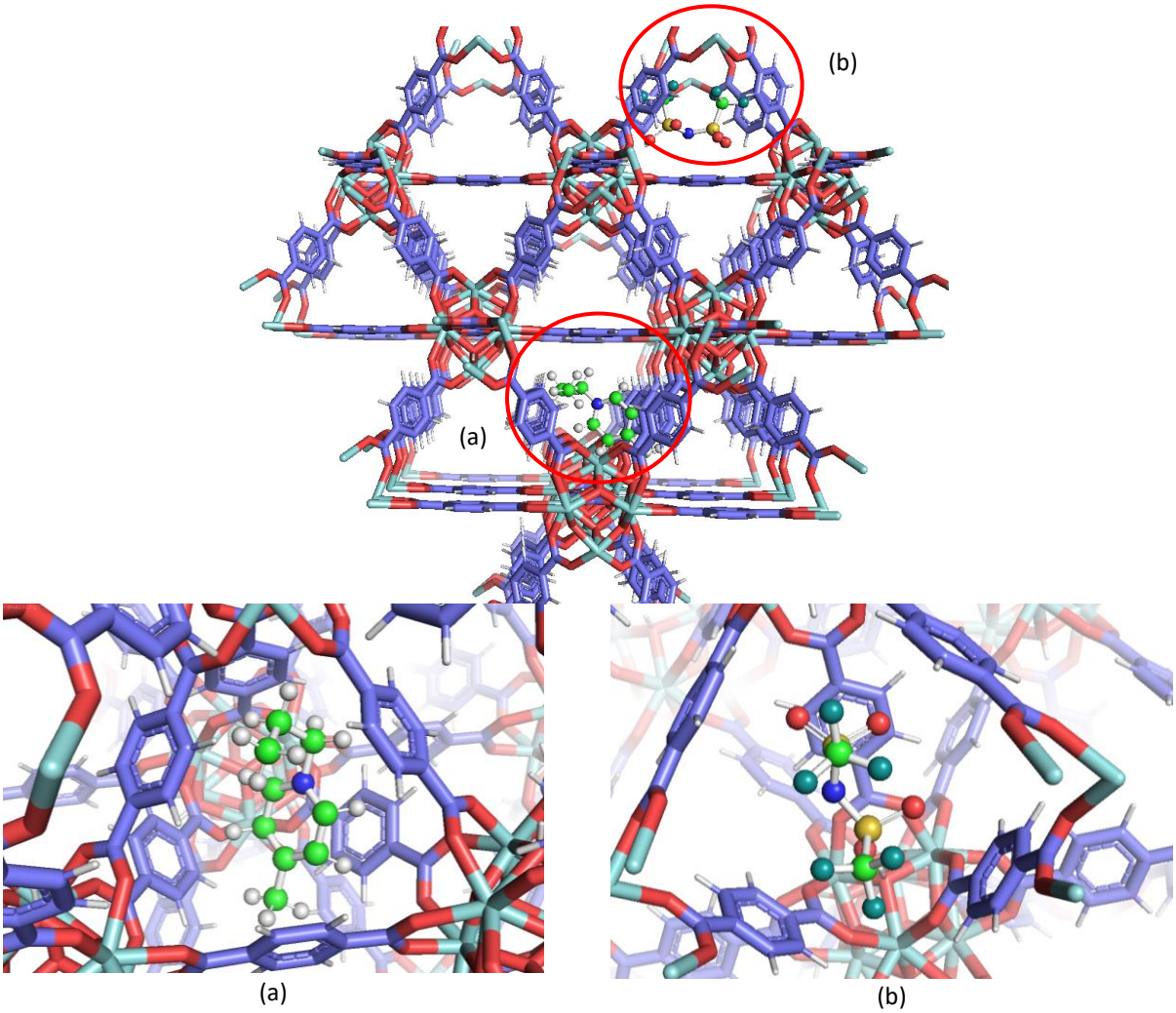

Fig. 4. The molecular docking structure of PMPYDM/TFSI-UIO66 (a) PMPYDM cation (b) TFSI anion

4. Conclusion

The topological properties of ILs and the binding energies interaction ILs-MOFs were investigated by carried out DFT calculation and molecular docking calculations respectively. From the MEP surface, both imidazole and pyridinium are shaded with the blue color which indicates the distribution of positive electrostatic potential, while the red color (negative potential) is distributed on the TFSI structure. The results were used as a reference for the possible location of ILs interaction inside UIO66 pores. The TFSI-imidazole and TFSI-pyridinium-based IL were successfully docked into UIO66. These matched ILs and MOFs have shown encouraging findings in terms of their capacity to bind to one another, demonstrating that the PMPYDM-TFSI has the greatest interaction with UIO66 (-8.60 kcal mol^{-1}). The results from binding energies show that the incorporation of both imidazole-TFSI and pyridinium-TFSI based ILs enhances the stability of the UIO6. Further investigation on the dynamic interaction between ILs and MOFs will be discussed in depth and will be disclosed in the next paper.

Acknowledgment
The authors are thankful to the Ministry of Education for the Fundamental Research Grant Scheme (FRGS/1/2020/STG04/UTP/02/3) to carry out this project.

References

[1] Jawed, A., V. Saxena, and L. M. Pandey. "Engineered nanomaterials and their surface functionalization for the removal of heavy metals: a review. J Water Process Eng 33: 101009." (2019). https://doi.org/10.1016/j.jwpe.2019.101009

[2] Wadhawan, S., A. Jain, J. Nayyar, and S. K. Mehta. "Role of nanomaterials as adsorbents in heavy metal ion removal from waste water: a review. J Water Process Eng 33: 101038." (2019). https://doi.org/10.1016/j.jwpe.2019.101038

[3] Liu, Qiming, Yi Zhou, Jian Lu, and Yanbo Zhou. "Novel cyclodextrin-based adsorbents for removing pollutants from wastewater: A critical review." *Chemosphere* 241 (2020): 125043. https://doi.org/10.1016/j.chemosphere.2019.125043

[4] Feng, Yi, Qian Chen, Minqi Jiang, and Jianfeng Yao. "Tailoring the properties of UiO-66 through defect engineering: A review." *Industrial & Engineering Chemistry Research* 58, no. 38 (2019): 17646-17659. https://doi.org/10.1016/j.chemosphere.2018.06.114

[5] Kobielska, Paulina A., Ashlee J. Howarth, Omar K. Farha, and Sanjit Nayak. "Metal–organic frameworks for heavy metal removal from water." *Coordination Chemistry Reviews* 358 (2018): 92-107. https://doi.org/10.1016/j.ccr.2017.12.010

[6] Peng, Yaguang, Hongliang Huang, Yuxi Zhang, Chufan Kang, Shuangming Chen, Li Song, Dahuan Liu, and Chongli Zhong. "A versatile MOF-based trap for heavy metal ion capture and dispersion." *Nature communications* 9, no. 1 (2018): 187. https://doi.org/10.1038/s41467-017-02600-2

[7] Wang, Chenghong, Xinlei Liu, J. Paul Chen, and Kang Li. "Superior removal of arsenic from water with zirconium metal-organic framework UiO-66." *Scientific reports* 5, no. 1 (2015): 16613. https://doi.org/10.1038/srep16613

[8] Rivera, José María, Susana Rincón, Cherif Ben Youssef, and Alejandro Zepeda. "Highly efficient adsorption of aqueous Pb (II) with mesoporous metal-organic framework-5: an equilibrium and kinetic study." *Journal of Nanomaterials* 2016 (2016). https://doi.org/10.1155/2016/8095737

[9] Li, Xiang, Bo Wang, Yuhua Cao, Shuang Zhao, Hang Wang, Xiao Feng, Junwen Zhou, and Xiaojie Ma. "Water contaminant elimination based on metal–organic frameworks and perspective on their industrial applications." *ACS Sustainable Chemistry & Engineering* 7, no. 5 (2019): 4548-4563. https://doi.org/10.1021/acssuschemeng.8b05751

[10] Aijaz, Arshad, and Qiang Xu. "Catalysis with metal nanoparticles immobilized within the pores of metal–organic frameworks." *The journal of physical chemistry letters* 5, no. 8 (2014): 1400-1411. https://doi.org/10.1021/jz5004044

[11] Kumar, K. Vasanth, Kathrin Preuss, Maria-Magdalena Titirici, and Francisco Rodríguez-Reinoso. "Nanoporous materials for the onboard storage of natural gas." *Chemical reviews* 117, no. 3 (2017): 1796-1825. https://doi.org/10.1021/acs.chemrev.6b00505

[12] Herm, Zoey R., Eric D. Bloch, and Jeffrey R. Long. "Hydrocarbon separations in metal–organic frameworks." *Chemistry of Materials* 26, no. 1 (2014): 323-338. https://doi.org/10.1021/cm402897c

[13] Huang, Wei, Shuo Li, Xianyi Cao, Chengyi Hou, Zhen Zhang, Jinkui Feng, Lijie Ci, Pengchao Si, and Qijin Chi. "Metal–organic framework derived iron sulfide–carbon core–shell nanorods as a conversion-type battery material." *ACS Sustainable Chemistry & Engineering* 5, no. 6 (2017): 5039-5048. https://doi.org/10.1021/acssuschemeng.7b00430

[14] Wiers, Brian M., Maw-Lin Foo, Nitash P. Balsara, and Jeffrey R. Long. "A solid lithium electrolyte via addition of lithium isopropoxide to a metal–organic framework with open metal sites." *Journal of the American Chemical Society* 133, no. 37 (2011): 14522-14525. https://doi.org/10.1021/ja205827z

[15] Polat, H. Mert, Muhammad Zeeshan, Alper Uzun, and Seda Keskin. "Unlocking CO2 separation performance of ionic liquid/CuBTC composites: Combining experiments with molecular simulations." *Chemical Engineering Journal* 373 (2019): 1179-1189. https://doi.org/10.1016/j.cej.2019.05.113

[16] Kavak, Safiyye, H. Mert Polat, Harun Kulak, Seda Keskin, and Alper Uzun. "MIL-53 (Al) as a Versatile Platform for Ionic-Liquid/MOF Composites to Enhance CO2 Selectivity over CH4 and N2." *Chemistry–An Asian Journal* 14, no. 20 (2019): 3655-3667. https://doi.org/10.1002/asia.201900634

[17] Kinik, F. Pelin, Cigdem Altintas, Volkan Balci, Burak Koyuturk, Alper Uzun, and Seda Keskin. "[BMIM][PF6] incorporation doubles CO2 selectivity of ZIF-8: elucidation of interactions and their consequences on performance." *ACS Applied Materials & Interfaces* 8, no. 45 (2016): 30992-31005. https://doi.org/10.1021/acsami.6b11087

[18] Zhang, Shiguo, Jiaheng Zhang, Yan Zhang, and Youquan Deng. "Nanoconfined ionic liquids." *Chemical Reviews* 117, no. 10 (2017): 6755-6833. https://doi.org/10.1021/acs.chemrev.6b00509

[19] Malde, Alpeshkumar K., Le Zuo, Matthew Breeze, Martin Stroet, David Poger, Pramod C. Nair, Chris Oostenbrink, and Alan E. Mark. "An automated force field topology builder (ATB) and repository: version 1.0." *Journal of chemical theory and computation* 7, no. 12 (2011): 4026-4037. https://doi.org/10.1021/ct200196m

[20] Morris, G. M., R. Huey, W. Lindstrom, M. F. Sanner, and R. K. Belew. "DS Goodsell i AJ Olson." *Journal of computational chemistry* 30 (2009): 2785-2791. https://doi.org/10.1002/jcc.21256
[21] Fuhrmann, Jan, Alexander Rurainski, Hans-Peter Lenhof, and Dirk Neumann. "A new Lamarckian genetic algorithm for flexible ligand-receptor docking." *Journal of computational chemistry* 31, no. 9 (2010): 1911-1918. https://doi.org/10.1002/jcc.21478
[22] Frisch, M. J., G. W. Trucks, H. B. Schlegel, G. E. Scuseria, M. A. Robb, J. R. Cheeseman, G. Scalmani et al. "Gaussian 16 Rev. C. 01, Wallingford, CT." *Wallingford, CT* (2016). https://doi.org/10.5965/1984723816322015001
[23] Tian Lu, FeiwuChen. "Multiwfn: A Multifunctional Wavefunction Analyzer." *J. Comput., and Chem* 33 (2012). https://doi.org/10.1002/jcc.22885
[24] Noorizadeh, Siamak, and Ehsan Shakerzadeh. "Shannon entropy as a new measure of aromaticity, Shannon aromaticity." *Physical Chemistry Chemical Physics* 12, no. 18 (2010): 4742-4749. https://doi.org/10.1039/b916509f
[25] Murray, J. S., and P. Politzer. "The electrostatic potential: an overview. WIREs Comput Mol Sci 1: 153–163." (2011). https://doi.org/10.1002/wcms.19
[26] Kruszewski, J., and T. M. Krygowski. "Definition of aromaticity basing on the harmonic oscillator model." *Tetrahedron Letters* 13, no. 36 (1972): 3839-3842. https://doi.org/10.1016/S0040-4039(01)94175-9
[27] Aleksić, Jovana, Milovan Stojanović, and Marija Baranac-Stojanović. "Aromaticity study of singlet-and triplet-state corannulene dianion and dication." *Journal of Physical Organic Chemistry* 36, no. 1 (2023): e4434. https://doi.org/10.1002/poc.4434
[28] Tarı, Gonca Özdemir, and Ercan Aydemir. "Experimental and DFT study of (E)-4-bromo-2 (((3-chloro-4-(4-chlorophenoxy) phenyl) imino) methyl)-5-fluorophenol: Molecular and electronic properties in solvent media." *Journal of Molecular Structure* 1277 (2023): 134880. https://doi.org/10.1016/j.molstruc.2022.134880
[29] Khazali, Mahsa, Morteza Rouhani, and Hamid Saeidian. "Utilizing the synergistic effect between imidazole aromaticity and guanidine structure for the computational design of novel uncharged organic superbases." *Journal of Molecular Structure* 1273 (2023): 134348. https://doi.org/10.1016/j.molstruc.2022.134348
[30] Wu, Chongchong, Alex De Visscher, and Ian D. Gates. "Comparison of electronic and physicochemical properties between imidazolium-based and pyridinium-based ionic liquids." *The Journal of Physical Chemistry B* 122, no. 26 (2018): 6771-6780. https://doi.org/10.1021/acs.jpcb.8b00764
[31] Abdullah, Nor Ain Fathihah, Khairulazhar Jumbri, and Nurul Yani Rahim. "Interaction of TFSI-Imidazole and TFSI-Pyridinium ILs with MOFs from Molecular Docking Simulation." In *Proceedings of the 6th International Conference on Fundamental and Applied Sciences: ICFAS 2020*, pp. 185-194. Springer Singapore, 2021. https://doi.org/10.1007/978-981-16-4513-6_16
[32] Abdullah, Nor Ain Fathihah, and Lee Sin Ang. "Binding sites of deprotonated citric acid and ethylenediaminetetraacetic acid in the chelation with Ba2+, Y3+, and Zr4+ and their electronic properties: a density functional theory study." *Acta Chimica Slovenica* 65, no. 1 (2018): 231-238. https://doi.org/10.17344/acsi.2017.3890
[33] Chen, Yifei, Zhongqiao Hu, Krishna M. Gupta, and Jianwen Jiang. "Ionic liquid/metal–organic framework composite for CO2 capture: a computational investigation." *The Journal of Physical Chemistry C* 115, no. 44 (2011): 21736-21742. https://doi.org/10.1021/jp208361p
[34] Gupta, Krishna M., Yifei Chen, Zhongqiao Hu, and Jianwen Jiang. "Metal–organic framework supported ionic liquid membranes for CO 2 capture: anion effects." *Physical Chemistry Chemical Physics* 14, no. 16 (2012): 5785-5794. https://doi.org/10.1039/c2cp23972h
[35] Li, Zhengjie, Yuanlong Xiao, Wenjuan Xue, Qingyuan Yang, and Chongli Zhong. "Ionic liquid/metal–organic framework composites for H2S removal from natural gas: a computational exploration." *The Journal of Physical Chemistry C* 119, no. 7 (2015): 3674-3683. https://doi.org/10.1021/acs.jpcc.5b00019